

Banner appropriate to article type will appear here in typeset article

# Turbulence teaches equivariance to neural networks

Ryley McConkey<sup>1</sup>†, Julia Balla<sup>1</sup>, Jeremiah Bailey<sup>1</sup>, Ali Backour<sup>1</sup>, Elyssa Hofgard<sup>1</sup>, Tommi Jaakkola<sup>1</sup>, Abigail Bodner<sup>1</sup>, and Tess Smidt<sup>1</sup>

<sup>1</sup>Massachusetts Institute of Technology, 77 Massachusetts Avenue, Cambridge, MA 02139-4301, United States.

(Received xx; revised xx; accepted xx)

We investigate how the rotational nature of turbulence affects learned mappings between quantities governed by the Navier-Stokes equations. By varying the degree of anisotropy in a turbulence dataset, we explore how statistical symmetry affects these mappings. To do this, we train super-resolution models at different wall-normal locations in a channel flow, where anisotropy varies naturally, and test their generalization. By evaluating the learned mappings on new coordinate frames and new flow conditions, we find that coordinate-frame generalization is a key part of the generalization problem. Turbulent flows naturally present a wide range of local orientations, so respecting the symmetries of the Navier-Stokes equations improves generalization to new flows. Importantly, turbulence's rotational structure can embed these symmetries into learned mappings—an effect that strengthens with isotropy and dataset size. This is because a more isotropic dataset samples a wider range of orientations, more fully covering the rotational symmetries of the Navier-Stokes equations. The dependence on isotropy means equivariance error is also scale-dependent, consistent with Kolmogorov's hypothesis. Therefore, turbulence provides its own data augmentation (we term this *implicit data augmentation*). We expect this effect to apply broadly to learned mappings between tensorial flow quantities, making it relevant to most machine learning applications in turbulence.

## 1. Introduction

Turbulence is characterized by coherent, rotating eddies across a wide range of scales. An ensemble of turbulence realizations defines a probability distribution over flow states, and this probability distribution can itself possess symmetries. In isotropic turbulence, while any single realization lacks rotational symmetry, the ensemble is rotationally invariant, providing complete statistical coverage over all rotations under which the Navier-Stokes equations are covariant. In this sense, the distributional symmetry thus matches the symmetry of the governing equations. Given the growing interest in data-driven emulators of the Navier-Stokes equations, this correspondence raises two questions. Can turbulence itself impart the symmetries of the underlying dynamics to learned mappings? Conversely, do models that better capture these symmetries generalize better to new distributions?

These questions strike at how the inherent nature of turbulence affects learned mappings between quantities arising from the Navier-Stokes equations. Data-driven turbulence closure models, accelerated solvers, and super-resolution models are all motivated by the immense

† Email address for correspondence: rmcconke@mit.edu

computational cost of simulating turbulence. Such approaches promise significant speedups, thereby enabling progress in physics and engineering applications involving turbulence. However, the accuracy, generalizability, and trust placed in these models strongly depend on their physical consistency with the Navier-Stokes equations.

Emulating the Navier-Stokes equations in a physically consistent way requires matching symmetries. *Equivariance* is often an important property in machine learning for physics, as it ensures that models respect the symmetries of the underlying system. An equivariant model  $f$  satisfies  $f(g \cdot x) = g \cdot f(x)$ , where  $g$  is a given element of a symmetry group (such as a rotation), and  $x$  is an input quantity. An equivariant model's outputs transform consistently with its inputs, matching the covariance of the physical system. Efforts have been made in nearly all domains of machine learning for turbulence to embed equivariance into machine learning models. For example, in turbulence closure modelling for Reynolds-averaged Navier-Stokes (RANS) problems, the commonly used Tensor Basis Neural Network (TBNN) achieves equivariance by predicting invariant coefficients of basis tensors that transform with  $g$  (Ling *et al.* 2016). In large eddy simulation (LES), example strategies for embedding equivariance involve predicting invariant scalars (Kurz *et al.* 2025) or transforming into the eigenframe of the strain-rate tensor (Prakash *et al.* 2022).

We select super-resolution as a representative task for machine learning in turbulence. Super-resolution (SR) with machine learning has become a promising method to augment numerical simulations of turbulence, by boosting the effective resolution of expensive calculations (Duraisamy *et al.* 2019). In this setting, convolutional neural networks (CNNs) have been widely applied to reconstruct velocity and vorticity fields from coarse inputs (Fukami *et al.* 2019; Liu *et al.* 2020; Fukami *et al.* 2024; Pang *et al.* 2024). Complementary approaches span models that incorporate temporal coherence and dynamics-aware training objectives (Fukami *et al.* 2021; Page 2025), as well as generative methods such as generative adversarial networks (GANs) (Nista *et al.* 2024) or diffusion models that reproduce realistic spectra and scaling laws (Shu *et al.* 2023; Whittaker *et al.* 2024; Fan *et al.* 2025). These methods do not enforce rotational equivariance explicitly, making super-resolution an ideal test-bed to investigate how symmetries can emerge from turbulence data alone.

Another way to encourage equivariance is via *explicit* data augmentation. The objective of explicit data augmentation is to generate distributional symmetry, which is in turn imparted onto the mapping. Input/output pairs are randomly transformed during training, by sampling members of the desired symmetry group. In this work, we show that turbulence can achieve this effect *implicitly*. In principle, a completely isotropic turbulence dataset knows no coordinate frame. In the infinite data limit, a model trained on a completely isotropic turbulence dataset should learn the rotational symmetries of the Navier-Stokes equations, having encountered similar structures in infinitely many orientations. Therefore, turbulence itself can produce an effect that often needs to be explicitly enforced in learned mappings.

In this study, we demonstrate two complementary results arising from the nature of turbulence. First, mappings which better respect rotational symmetries of the Navier-Stokes equations generalize better to new flows (Section 3.1). This reflects a fundamental aspect of turbulence: since turbulent flows contain structures in widely varying orientations, models that cannot generalize across coordinate frames will struggle with unseen configurations. Second, the rotational nature of turbulence itself imparts rotational equivariance to learned mappings. Therefore, turbulence itself provides a form of *implicit data augmentation* arising from the distributional symmetry of the flow. This implicit data augmentation depends on the size and isotropy of the training dataset (Section 3.2), and is scale-dependent, consistent with Kolmogorov's hypothesis of local isotropy at small scales (Section 3.3). We quantify the learned equivariance via the equivariance error (Section 2.1), which measures the degree to which a model respects the rotational symmetries of the Navier-Stokes equations.

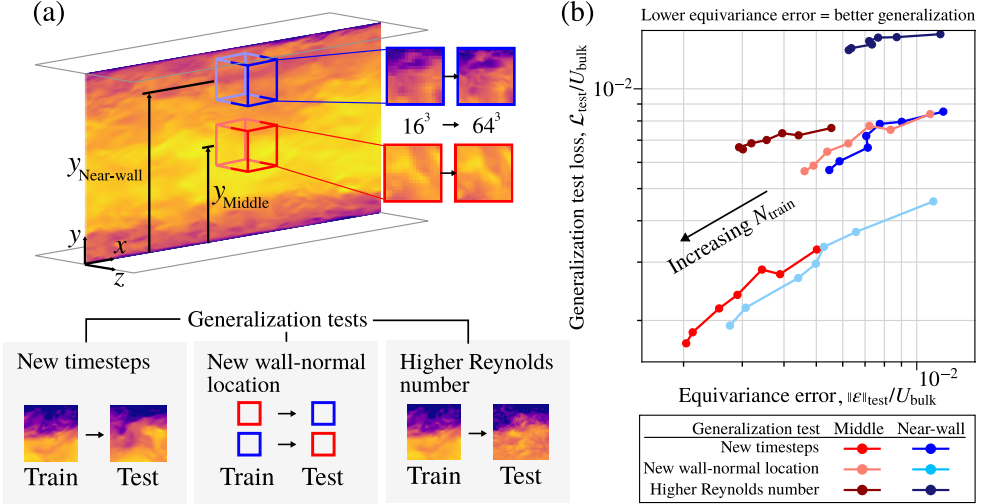


Figure 1: (a) Approximate location of the two sub-boxes (near-wall and middle) in the turbulent channel flow, and (b) test loss vs equivariance error for three generalization tasks: extrapolating in time, extrapolating to a new level of anisotropy (by changing the wall-normal location), and generalizing to a  $5\times$  increase in Reynolds number (single box, explicit augmentation). Colour in (b) is by training dataset. Across all models and training configurations, there is a consistently high correlation between a model’s ability to generalize to new coordinate frames (equivariance error), and generalization error.

## 2. Methodology

For a representative turbulence dataset, we select the canonical turbulent channel flow. In this flow, rotating eddies of various scales pass through the domain and are influenced anisotropically by the presence of the top and bottom walls. The degree of anisotropy varies with the wall-normal direction: near the wall, flow is highly anisotropic. In the center of the channel, the flow is still anisotropic but to a much lower degree. Choosing turbulent channel flow allows us to vary the degree of isotropy in the training dataset by sub-sampling the domain. However, we are still able to make direct comparisons between different sub-sampled regions of the flow, since the fields come from the same flow. Specifically, we use the Johns Hopkins turbulent channel flow dataset at friction Reynolds number  $Re_\tau = 1000$  (Li *et al.* 2008). This moderately turbulent Reynolds number produces rotating eddies of various sizes in the channel. This dataset features a high resolution in both space and time, allowing us to explore the effect of adding more data in both of these dimensions. In Section 3.1, we test generalization up to  $Re_\tau = 5200$  from the same database (Li *et al.* 2008).

In two distinct regions of the flow, we take three sub-boxes each, creating an ensemble of six boxes total. The two regions correspond to the middle of the channel and the near-wall region. Figure 1 shows the locations of the two regions, and an example super-resolution task. Figure 2 shows how the degree of anisotropy varies between the two selected  $y$  coordinates. All three boxes from a distinct region have the same central  $y$  coordinate. Given that turbulent channel flow is statistically stationary, ergodic and homogeneous at a fixed  $y$ , additional samples in time and additional boxes (at fixed  $y$ ) simply add data from a given ensemble of identically distributed turbulence realizations.

### 2.1. Equivariance error

We define *equivariance error* in order to quantify how well a model has learned equivariance (Wang *et al.* 2022). A perfectly equivariant model automatically transforms its outputs

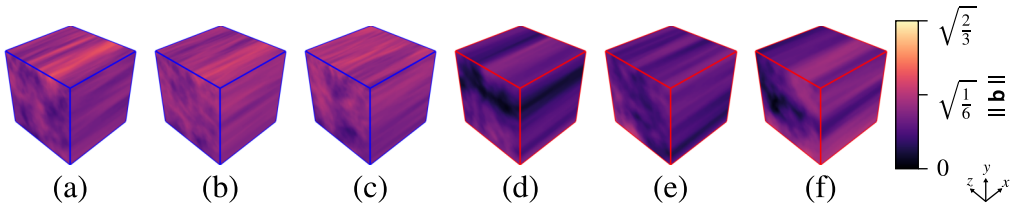


Figure 2: Anisotropy tensor magnitude for the three sub-boxes in the near-wall (blue) and middle (red) locations in the channel. The  $\sqrt{2/3}$  bound represents the one-component limit (Banerjee *et al.* 2007). The near-wall region is more anisotropic due to the proximity of the wall.

when the inputs transform. Formally, given input  $x$ , group  $G$ , and group elements  $g \in G$ , a model  $f$  is  $G$ -equivariant if  $f(g \cdot x) = g \cdot f(x) \forall g \in G$ . We define the pointwise equivariance error as the absolute residual of the definition of equivariance:

$$\mathbf{E}(\mathbf{x}_n; g) = |\mathbf{f}(g \cdot \mathbf{x}_n) - g \cdot \mathbf{f}(\mathbf{x}_n)| \quad (2.1)$$

where  $\mathbf{E}(\mathbf{x}_n; g)$  is the equivariance error for a given group element  $g$  and coarsened velocity vector field  $\mathbf{x}_n$ ,  $n$  indexes the dataset, and  $\mathbf{f}$  is the learned super-resolution function (a vector-valued function).

In this context,  $\mathbf{E}(\mathbf{x}_n; g)$  is the component-wise absolute difference between two vector fields and is therefore a sign-fixed vector field. At each field point, it measures how close the mapping  $\mathbf{f}$  is to being perfectly equivariant under a given group element  $g$  for the input  $\mathbf{x}$ . We can collapse this vector field to generate integral quantities by taking the average over all group elements, data points, and field points. The average equivariance error norm is calculated as

$$\|\varepsilon\| = \frac{1}{|G|N} \sum_{g \in G} \sum_{n=1}^N \|\mathbf{E}(\mathbf{x}_n; g)\| \quad (2.2)$$

where  $N$  is the dataset size,  $|G|$  is the cardinality of the group, and  $\|\cdot\|$  is the  $L^2$  norm.  $\|\varepsilon\|$  is a single measure of how perfectly equivariant a vector-valued model is.

It should be noted that equivariance error does not depend at all on *how well* a model performs with respect to the ground truth data—it only depends on how equivariant the model is. Therefore, it can be measured for any model without ground truth data. In this investigation, we show that equivariance error correlates with performance on ground truth data due to the nature of turbulence.

### 2.1.1. Discrete vs continuous rotation groups

In this work, we focus specifically on data augmentation using the rotational octahedral group  $O$ . We select this discrete group rather than the rotational one for several reasons. Numerical simulation data only embeds the discrete symmetries of the Navier-Stokes equations, since discretization error depends on the alignment of the flow with the grid. Therefore, it is inappropriate to assess if a model can learn a continuous rotation group from data which does not contain this symmetry. Further, additional error is introduced when explicitly augmenting data using a continuous rotation group, since the data needs to be interpolated onto a transformed grid (Yasuda & Onishi 2023). Since our grid is uniform, we introduce no interpolation error when transforming using group elements of  $O$ .  $O$  contains 24 rotation group elements in three dimensions. Using the discrete group  $G = O$ , in Equation 2.2 we have  $|G| = 24$ , and  $g \in O$  are the 24 octahedral rotations (we leave the investigation of reflections and inversions to future work).

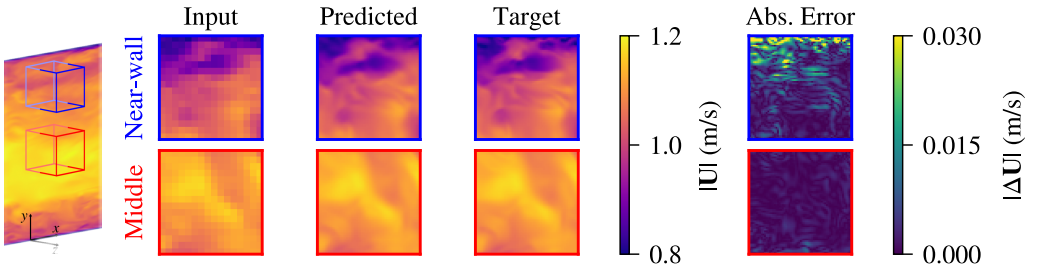


Figure 3: Example outputs from the CNN (1500 samples, single box, rotational augmentation). Colour here is by velocity magnitude, but the models super-resolve each velocity component separately.

## 2.2. Dataset and model details

The dataset used consists of a variety of turbulent channel flow ensembles. The aim of the dataset is to explore various methods of ensembling turbulence realizations. We generate these ensembles using both a single time series (temporal ensembling), and combining multiple times series from multiple sub-boxes (spatio-temporal ensembling). We split the Johns Hopkins channel flow dataset (Li *et al.* 2008) of 4000 snapshots over approximately one flow-through time sequentially into a training set (67%), validation set (20%), and test set (13%). We sub-sample six square boxes of side length  $0.6H$ , three of which have centers at  $y_{\text{Near-wall}} = 1.65H$  and three of which have centers at  $y = H$ , where  $H$  is the channel half-height. We randomly choose  $x$  and  $z$  coordinates in the channel for the three boxes. We explore randomly selected subsets of the training dataset in Section 3, including randomly sampling the time series from a single-box dataset (temporal ensembling), and a three-box dataset (spatio-temporal ensembling).

In this work, we select a simple and representative super-resolution model (Dong *et al.* 2016). Specifically, we use a compact multi-scale convolutional super-resolution network that upsamples a low-resolution velocity field volume  $\mathbf{x} \in \mathbb{R}^{3 \times D \times H \times W}$  to the target high-resolution  $\mathbf{U} \in \mathbb{R}^{3 \times sD \times sH \times sW}$ . Upsampling by factor  $s$  is implemented as a sequence of resize-then-refine stages, one for each factor of 2. At each stage, the input is upsampled through trilinear interpolation and passed through two convolutional layers. A final convolution projects the features to 3 output channels, yielding the super-resolved prediction. We use reflection padding on all image edges. The SR model is trained to minimize the mean absolute error (MAE) loss between the ground truth and predicted high-resolution fields, which has been shown to better preserve perceptual quality and reduce oversmoothing compared to mean squared error (MSE) loss in image restoration tasks (Zhao *et al.* 2017).

We fix the CNN architecture and hyperparameters for all of our experiments. The network contains two successive upsampling layers, each enlarging the input by a factor of 2, resulting in an overall scale factor of  $s = 4$ . 3D Convolutions use kernels of size 3 with reflection padding of one pixel on each side, followed by ReLU activations. All hidden layers have 128 channels. Models are trained with the Adam optimizer with learning rate  $6 \times 10^{-4}$  and batch size of 32. We train each model for 3000 epochs and take the model which has the lowest validation loss over all epochs. The required epochs for training convergence increased with the number of training points. However, we observed that the training converged for all models and datasets within the 3000 epoch range.

All code used in this study is available on GitHub: <https://github.com/atomicarchitects/turbulence-implicit-augmentation> (McConkey *et al.* 2024). We include end-to-end steps to reproduce our results, model weights, and all code used to generate the plots in this manuscript.

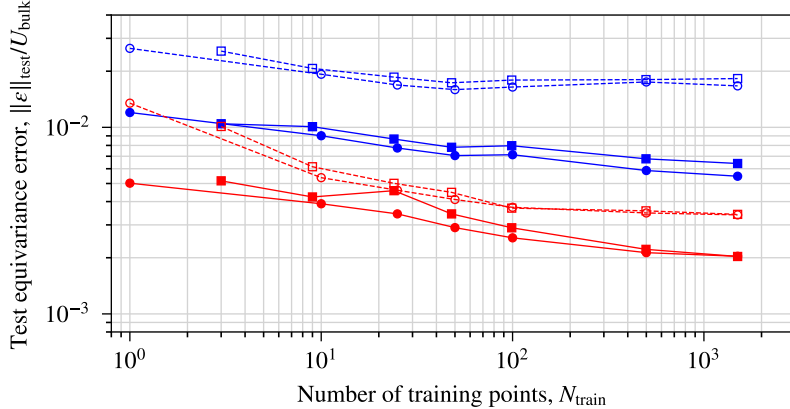


Figure 4: Test equivariance error vs number of training samples for various training configurations. While rotational augmentation reduces the equivariance error, adding more training samples also provides a degree of rotational data augmentation in turbulence.

### 3. Results

For a discussion of the distinction between *explicit* and *implicit* data augmentation and the rotational augmentation group used in this work, see Section 2. In Section 3, “augmentation” refers to explicit augmentation—we show that implicit augmentation occurs automatically. Specifically, when a training point is sampled from the original dataset, input/output pairs are randomly transformed with some group element  $g \in O$  (see Section 2.1 for more details).

Figure 3 shows a super-resolved test set example using a rotationally augmented model. Both the augmented and non-augmented models extrapolate well in time (in the original coordinate frame) after seeing 1500 examples from a given box.

#### 3.1. Generalizing to new flows

It is well known that in many applications of machine learning for turbulence, models struggle to generalize to new geometries, flow conditions, and Reynolds numbers (Duraisamy *et al.* 2019). The reasons for this are numerous: lack of sufficient data, distributional shift due to subtle changes in physics, and emergent phenomena that are not in the training dataset all frequently occur in turbulence. Here, we aim to investigate whether a model which is better able to capture the rotational symmetries of the Navier-Stokes equations generalizes better.

Figure 1 compares generalization losses (error) to equivariance error magnitude for three generalization tests. For all three generalization tests, there is a clear correlation between equivariance error and generalization error. The model trained on the near-wall dataset generalizes better to the middle of the channel than the reverse case. This asymmetry is likely due to the more isotropic middle distribution not generalizing well to the strongly anisotropic flow near the wall. All models feature a higher test loss when generalizing to the higher Reynolds number channel flow. The models trained at  $Re_\tau = 1000$  have not seen the broader inertial range and higher levels of turbulence in the  $Re_\tau = 5200$  test dataset. Nevertheless, even for this challenging generalization test, there is still a correlation between equivariance error and generalization error for almost all models. It should be noted that the  $||\varepsilon_{\text{test}}||$  reported in Figure 1 is the test set equivariance error from the original time series for all three plots. In other words, Figure 1 shows the correlation between equivariance error on a model’s original test dataset (held out time-steps) and how well that model generalizes to a new turbulent flow.

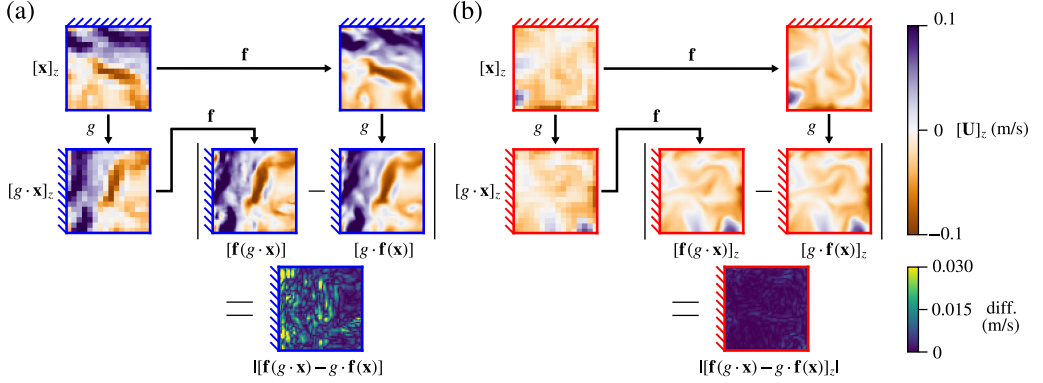


Figure 5: Example test set equivariance error field for the (a) near-wall and (b) middle datasets. We show the case of 1500 training examples from a single box, without any explicit data augmentation (i.e., implicit augmentation only). Hatching indicates the direction of the top wall for reference (not the wall boundary).  $[\cdot]_z$  denotes the  $z$ -component of a field. The  $z$  velocity component on an  $xy$  plane is shown, with  $g \equiv C_{4z}$  (a  $90^\circ$  rotation about the  $z$  axis). The  $z$  velocity component is not transformed by this rotation, so the transformed image appears as a straightforward rotation. Comparing the difference contours, we see that the model trained on the more isotropic mid-plane data (b) has a significantly lower equivariance error.

### 3.2. Implicit spatio-temporal data augmentation in turbulence

We show here that implicit spatio-temporal data augmentation occurs in turbulence. Simply put, with more examples of rotational turbulent flow, models can learn equivariance without explicit data augmentation. Figure 4 shows the trend of equivariance error vs. number of training data points for models with and without explicit data augmentation. In all cases, Figure 4 shows that the equivariance error decreases with number of training samples. The equivariance error magnitude is lower for more isotropic data, indicating that more isotropic datasets are more effective at providing implicit data augmentation. This trend is intuitive; a dataset which is completely isotropic contains complete distributional symmetry.

As we show in Section 3.1, generalization error decreases with equivariance error—therefore, it is desirable to have a model learn equivariance during training. While implicit data augmentation occurs with increasing training set size, Figure 4 shows that explicit data augmentation further reduces the equivariance error. Therefore, in a finite data regime, and with data that is not fully isotropic, it is still advantageous to explicitly augment the dataset. Figure 5 demonstrates that without explicit data augmentation, the model trained on the more isotropic middle of the channel features a significantly lower equivariance error.

### 3.3. Scale-dependence of learned equivariance

Kolmogorov's local isotropy hypothesis states that small-scale motions recover statistical isotropy when the Reynolds number is sufficiently high (Kolmogorov 1991). In Section 3.2, we show that a more isotropic dataset leads to lower equivariance error. Here, we show that when combined with Kolmogorov's hypothesis, this isotropy-based phenomenon leads to a scale-dependence of the equivariance error.

Figure 6 shows the one-dimensional power spectra of the equivariance error vector. For all cases, there is a falloff of equivariance error with scale, which aligns with Kolmogorov's hypothesis of increasing isotropy as eddies break up into smaller and smaller motions in turbulence. Without explicit data augmentation, the falloff continues even into the small scales. With explicit data augmentation, the trend flattens out towards the smaller scales.

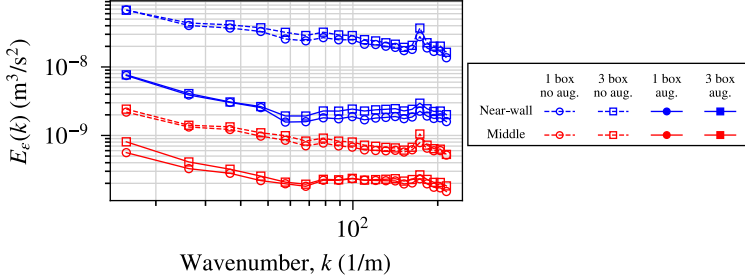


Figure 6: One-dimensional equivariance error power spectra for various training configurations. Equivariance error drops off with scale for all datasets and training configurations, due to increasing isotropy with decreasing scale (Kolmogorov’s hypothesis).

All cases show a sharp peak in the equivariance error power spectra at a wavenumber  $k \approx 180$ . This peak occurs past the end of the input wavenumber. Implicit data augmentation only occurs for wavenumbers that are resolved in the model inputs. Past this value ( $k \approx 90$ ), the model is super-resolving in spectral space. Interestingly, this peak appears at roughly the second harmonic of the cutoff wavenumber. The reason for this peak in the equivariance error power spectra is unknown and will be investigated in future work.

These results confirm findings of the previous work by Wang *et al.* (2024), which demonstrated that a symmetry-breaking model learns scale-dependent symmetry-breaking weights. Our results confirm this from a top-down viewpoint. While we show that a single model learns scale-dependent equivariance, Wang *et al.* (2024) showed that models trained on scale-dependent data learn different symmetry-breaking weights. Both investigations demonstrate that models learn scale-dependent equivariance, due to the scale-dependent nature of isotropy in a turbulent flow. However, the peak in the spectra observed in Figure 6 was not observed in Wang *et al.* (2024). This difference means that the nature of this peak arises from training on multiple scales of turbulence simultaneously, as Wang *et al.* (2024) scale-separated all training data *a priori*.

#### 4. Conclusion

We demonstrated that the degree of anisotropy influences the degree to which the model learns equivariance. Models trained on the near-wall flow consistently feature higher equivariance error, and require more explicit data augmentation to learn equivariance compared to models trained on the channel mid-plane. Further, taking the power spectrum of the equivariance error reveals that the largest scales have the highest equivariance error. This scale-dependence agrees with Kolmogorov’s hypothesis: the largest scales of turbulence are more anisotropic than the smaller scales in channel flow.

Though we selected super-resolution in this work, we believe these results also extend to other applications of machine learning in turbulence. Future investigations will examine how implicit data augmentation occurs in machine learning for subgrid scale modelling; early results demonstrate that similar behaviour occurs as seen in the present super-resolution work. These results lead us to postulate that learned mappings between quantities in a turbulent flow field will be subject to implicit data augmentation.

Our results inform several future directions in the application of machine learning for turbulence. The field-wide problem of generalizability has sparked massive interest, given current poor performance (Duraisamy *et al.* 2019). Here, we demonstrated consistent correlation

between generalization error and equivariance error in Figure 1(b). This correlation reveals that a model’s ability to generalize to new coordinate frames and match the symmetries of the Navier-Stokes equations is correlated with its ability to generalize to new turbulent flows. By simply improving the ability of the model to generalize to a new coordinate frame, we can promote better generalization to new turbulent flows. Lastly, the present work raises a concern with the use of large, statistically stationary, and isotropic datasets to prove new machine learning methodologies. Training under these ideal conditions can easily promote an overly optimistic viewpoint of new methodologies. Figure 1(b) shows that models trained under these conditions generalize poorly to more anisotropic flows. To remedy this, we suggest including anisotropic flows and using explicit data augmentation.

The results in Section 3.1 show a strong correlation between equivariance error and generalization error; this prompts the limit-taking question of how well a model with zero equivariance error generalizes. Future investigations will compare the role of equivariance as an inductive bias in the model. Exact equivariance can be imposed through various architectural approaches, such as group-equivariant convolutions and neural operators (Helwig *et al.* 2023; Xu *et al.* 2024). Inexact equivariance can also be achieved by regularizing models to transform consistently without altering their backbone (Bai *et al.* 2025; Raissi *et al.* 2019). We postulate that architectures with equivariance as an inductive bias will generally require less training data than non-equivariant ones; this result is known in other scientific machine learning domains. However, in the domain of turbulence, this is especially true, given the existence of implicit data augmentation demonstrated in this investigation.

**Funding.** We acknowledge the support of the National Science Foundation under Cooperative Agreement PHY-2019786 (The NSF AI Institute for Artificial Intelligence and Fundamental Interactions). J. Balla was supported by the Department of Defense (DoD) through the National Defense Science & Engineering Graduate (NDSEG) Fellowship Program. J. Bailey was supported by the MIT Summer Research Program (MSRP). EH was supported by the U.S. Department of Energy, Office of Science, Office of Advanced Scientific Computing Research, Department of Energy Computational Science Graduate Fellowship under Award Number DESC0024386. RM was supported by the Natural Sciences and Engineering Research Council of Canada (NSERC), the Thornton Family Fund, and the MIT Electrical Engineering and Computer Science Transformation Grant. This work was supported by the U.S. Department of Energy, National Nuclear Security Administration under Award Number DE-NA0004266. This research used resources of the MIT Office of Research Computing and Data.

**Declaration of interests.** The authors report no conflict of interest.

**Declaration of AI use.** AI tools were used to proofread the manuscript.

**Data availability statement.** The data and codes that support the findings of this study are openly available at <https://github.com/atomicarchitects/turbulence-implicit-augmentation>.

**Author ORCIDs.** R. McConkey, <https://orcid.org/0000-0003-0674-1849>; J. Balla, <https://orcid.org/0000-0001-6831-2877>; J. Bailey, <https://orcid.org/0000-0002-0436-9118>; A. Backour, <https://orcid.org/0009-0002-5330-3921>; E. Hofgard, <https://orcid.org/0000-0002-0745-9477>; T. Jaakkola, <https://orcid.org/0000-0003-1419-9236>; A. Bodner, <https://orcid.org/0000-0003-1333-2840>; T. Smidt, <https://orcid.org/0000-0001-5581-5344>

## REFERENCES

BAI, YUZHENG & OTHERS 2025 A regularization-guided equivariant approach for image restoration. In *Proceedings of the IEEE/CVF Conference on Computer Vision and Pattern Recognition*.

BANERJEE, S., KRAHL, R., DURST, F. & ZENGER, CH 2007 Presentation of anisotropy properties of turbulence, invariants versus eigenvalue approaches. *Journal of Turbulence* **8**, 1–27.

DONG, CHAO, LOY, CHEN CHANGE, HE, KAIMING & TANG, XIAOOU 2016 Image super-resolution using deep convolutional networks. *IEEE transactions on pattern analysis and machine intelligence* **38** (2), 295–307.

DURAISAMY, KARTHIK, IACCARINO, GIANLUCA & XIAO, HENG 2019 Turbulence modeling in the age of data. *Annual Review of Fluid Mechanics* **51** (Volume 51, 2019), 357–377.

FAN, XIANTAO, AKHARE, DEEPAK & WANG, JIAN-XUN 2025 Neural differentiable modeling with diffusion-based super-resolution for two-dimensional spatiotemporal turbulence. *Computer Methods in Applied Mechanics and Engineering* **433**, 117478.

FUKAMI, KAI, FUKAGATA, KOJI & TAIRA, KUNIHIKO 2019 Super-resolution reconstruction of turbulent flows with machine learning. *Journal of Fluid Mechanics* **870**, 106–120.

FUKAMI, KAI, FUKAGATA, KOJI & TAIRA, KUNIHIKO 2021 Machine-learning-based spatio-temporal super resolution reconstruction of turbulent flows. *Journal of Fluid Mechanics* **909**, A9.

FUKAMI, KAI, FUKAGATA, KOJI & TAIRA, KUNIHIKO 2024 Single-snapshot machine learning for super-resolution of turbulence. *Journal of Fluid Mechanics*.

HELWIG, JACOB, ZHANG, XUAN, FU, CONG, KURTIN, JERRY, WOJTOWYTSCH, STEPHAN & JI, SHUIWANG 2023 Group equivariant fourier neural operators for partial differential equations. In *International Conference on Machine Learning*.

KOLMOGOROV, A. N. 1991 The local structure of turbulence in incompressible viscous fluid for very large reynolds numbers. *Proceedings: Mathematical and Physical Sciences* **434** (1890), 9–13.

KURZ, MARIUS, BECK, ANDREA & SANDERSE, BENJAMIN 2025 Harnessing equivariance: Modeling turbulence with graph neural networks, arXiv: 2504.07741.

LI, YI, PERLMAN, ERIC, WAN, MINPING, YANG, YUNKE, MENEVEAU, CHARLES, BURNS, RANDAL, CHEN, SHIYI, SZALAY, ALEXANDER & EYINK, GREGORY 2008 A public turbulence database cluster and applications to study lagrangian evolution of velocity increments in turbulence. *Journal of Turbulence* **9**, 1–29.

LING, JULIA, KURZAWSKI, ANDREW & TEMPLETON, JEREMY 2016 Reynolds averaged turbulence modelling using deep neural networks with embedded invariance. *Journal of Fluid Mechanics* **807**, 155–166.

LIU, BO, TANG, JIUPENG, HUANG, HAIBO & LU, XI-YUN 2020 Deep learning methods for super-resolution reconstruction of turbulent flows. *Physics of Fluids* **32**, 025105.

MC CONKEY, RYLEY, BALLA, JULIA, BACKOUR, ALI & BAILEY, JEREMIAH 2024 <https://github.com/atomicarchitects/turbulence-implicit-augmentation>.

NISTA, LUDOVICO, PITSCHE, HEINZ, SCHUMANN, CHRISTOPH D. K., BODE, MATHIS, GRENGA, TEMISTOCLE, MACART, JONATHAN F. & ATTILI, ANTONIO 2024 Influence of adversarial training on super-resolution turbulence reconstruction. *Phys. Rev. Fluids* **9**, 064601.

PAGE, JACOB 2025 Super-resolution of turbulence with dynamics in the loss. *Journal of Fluid Mechanics*.

PANG, ZHENTAO, LIU, KAI, XIAO, HUALIN, JIN, TAI, LUO, KUN & FAN, JIANREN 2024 A deep-learning super-resolution reconstruction model of turbulent reacting flow. *Computers & Fluids* **275**, 106249.

PRAKASH, AVIRAL, JANSEN, KENNETH E. & EVANS, JOHN A. 2022 Invariant data-driven subgrid stress modeling in the strain-rate eigenframe for large eddy simulation. *Computer Methods in Applied Mechanics and Engineering* **399**, 115457.

RAISSI, M., PERDIKARIS, P. & KARNIADAKIS, G.E. 2019 Physics-informed neural networks: A deep learning framework for solving forward and inverse problems involving nonlinear partial differential equations. *Journal of Computational Physics* **378**, 686–707.

SHU, DULE, LI, ZI JIE & BARATI FARIMANI, AMIR 2023 A physics-informed diffusion model for high-fidelity flow field reconstruction. *Journal of Computational Physics* **478**, 111972.

WANG, RUI, HOFGARD, ELYSSA, GAO, HAN, WALTERS, ROBIN & SMIDT, TESS 2024 Discovering symmetry breaking in physical systems with relaxed group convolution. In *Proceedings of the 41st International Conference on Machine Learning* (ed. Ruslan Salakhutdinov, Zico Kolter, Katherine Heller, Adrian Weller, Nuria Oliver, Jonathan Scarlett & Felix Berkenkamp), *Proceedings of Machine Learning Research*, vol. 235, pp. 50599–50621. PMLR.

WANG, RUI, WALTERS, ROBIN & YU, ROSE 2022 Approximately equivariant networks for imperfectly symmetric dynamics, arXiv: 2201.11969.

WHITTAKER, T., NAIR, P. P. R., LIVESCU, D. & CHERTKOV, M. 2024 Turbulence scaling from deep learning diffusion generative models. *Journal of Computational Physics*.

XU, MINKAI, HAN, JIAQI, LOU, AARON, AZIZZADENESHELI, KAMYAR, ERMON, STEFANO & ANANDKUMAR, ANIMA 2024 Equivariant graph neural operator for modeling 3d dynamics. In *International Conference on Learning Representations*.

YASUDA, YUKI & ONISHI, RYO 2023 Rotationally equivariant super-resolution of velocity fields in two-dimensional fluids using convolutional neural networks. *APL Machine Learning*.

ZHAO, HANG, GALLO, ORAZIO, FROSIO, IURI & KAUTZ, JAN 2017 Loss functions for image restoration with neural networks. *IEEE Transactions on Computational Imaging* **3** (1), 47–57.